Polarimetry-based method to extract geometry-independent metrics of tissue anisotropy

Marika A. Wallenburg,[1] Michael F. G. Wood,[1] Nirmalya Ghosh,[2] and I. Alex Vitkin[1,3,*]

[1]*Ontario Cancer Institute, University Health Network, and Department of Medical Biophysics, University of Toronto, Toronto, Ontario, Canada M5G 2M9*

[2]*IISER Kolkata, Mohanpur Campus, PO: BCKV Campus Main Office, Mohanpur 741252, West Bengal, India*

[3]*Department of Radiation Oncology, University of Toronto, Toronto, Ontario, Canada M5G 2M9*

Corresponding author: vitkin@uhnres.utoronto.ca

Recently, we have used polarimetry as a method for assessing the linear retardance of infarcted myocardium. While linear retardance reflects tissue anisotropy, experimental geometry has a confounding effect due to dependence of the linear retardance on the orientation of the sample with respect to the probing beam. Here, polarimetry imaging of an 8 mm diameter birefringent polystyrene sphere of known anisotropy axis was used to test a dual-projection method by which the anisotropy axis and its true magnitude can be reconstructed, thus eliminating the confounding effect of anisotropy axis orientation. Feasibility is demonstrated in *ex-vivo* tissue imaging.   © 2010 Optical Society of America

OCIS codes: 170.0110, 170.3890, 170.6935.

Polarized light methods have recently shown promise for assessing microstructure and organization in biological tissues, for example, in skin [1,2], tendon [3], articular cartilage [4], and skeletal and cardiac muscle [5,6]. Anisotropic materials manifest different refractive indices along different axes, an effect known as birefringence. Tissue birefringence can be used as an indication of its organization state, as highly aligned molecules and structures, such as linear collagen and myocytes, will exhibit higher birefringence than structures with little anisotropy, such as disorganized scar tissue. It has previously been shown, for instance, that the birefringence of heart tissue decreases in the region of an infarct and partially rebounds following regenerative treatments [6,7]. Linear retardance δ was used as a measure of birefringence, $\Delta n = n_e - n_o$ (n_e and n_o are the refractive indices along the extraordinary and ordinary axes, respectively), as the two are proportional: $\delta = (2\pi/\lambda) \times d\Delta n$, where d is the pathlength of photons and λ is the wavelength of light.

However, the apparent (measured) birefringence of the material, $\Delta n_{app} = n - n_o$ (where n is the apparent index of refraction), is not only a function of the degree of anisotropy of a material but also depends on experimental geometry [8]:

$$\frac{1}{n^2} = \frac{\cos^2 \varphi}{n_e^2} + \frac{\sin^2 \varphi}{n_o^2}, \tag{1}$$

where φ [Fig. 1(a)] is the elevation angle between the extraordinary (anisotropy) axis and the imaging plane (i.e., the plane perpendicular to the beam path). This effect interferes with the interpretation of the linear retardance as a direct indicator of a material's true anisotropy.

To resolve this ambiguity, we propose a dual-projection method, whereby a sample is imaged twice at different incident angles of the probing beam. The apparent linear retardance δ_{app} and azimuthal angle θ [the projection of the anisotropy axis in the imaging plane, Fig. 1(a)], measured with two different sample/beam geometries, provide sufficient information to reconstruct the true magnitude and orientation of a material's anisotropy, independent of experimental geometry effects. A similar approach has been used for polarization-sensitive optical coherence tomography by Ugryumova *et al.* [9]. To characterize the experimental performance of this reconstruction, we report a polarimetric study of an 8 mm diameter polystyrene sphere of known anisotropy axis.

The sphere was cut from a birefringent polystyrene cylinder. The anisotropy axis was along the cylinder axis, as visually confirmed with crossed polarizers. Polarimetry setup [Fig. 1(b)] has been described in detail elsewhere [7,10]; it determines the sample transfer function for polarized light interaction (the representation of which is a 4×4 Mueller matrix) by measuring the output polarization for different input polarizations. The incident light from a 635 nm diode laser (ThorLabs), was polarized either linearly or circularly, and each polarization state (linear or circular) of the outgoing beam was recorded by a CCD camera (Photometrics CoolSnap K4). Experiments were performed with the incoming beam at normal incidence [on axis, $\chi = 0°$ in Fig. 1(b)], or slightly angled (off axis, $\chi = 8°$), to avoid CCD saturation with light directly transmitted around the sample edges (of importance to subsequent tissue imaging). Mueller matrix decomposition, as described in [11], was performed to extract and quantify the linear retardance δ_{app} and the azimuthal angle θ, which were then averaged over all pixels in the image.

For each dual projection, imaging was done twice: with the sphere in its original position, and with the sphere rotated about its center by $15° \le \alpha \le 35°$ around the vertical (y) axis [Fig. 1(b)]. Equation (1) was used to determine the anisotropy magnitude and orientation that offered the best fit to both sets of measurements. Specifically, reexpressing the retardance using Eq. (1),
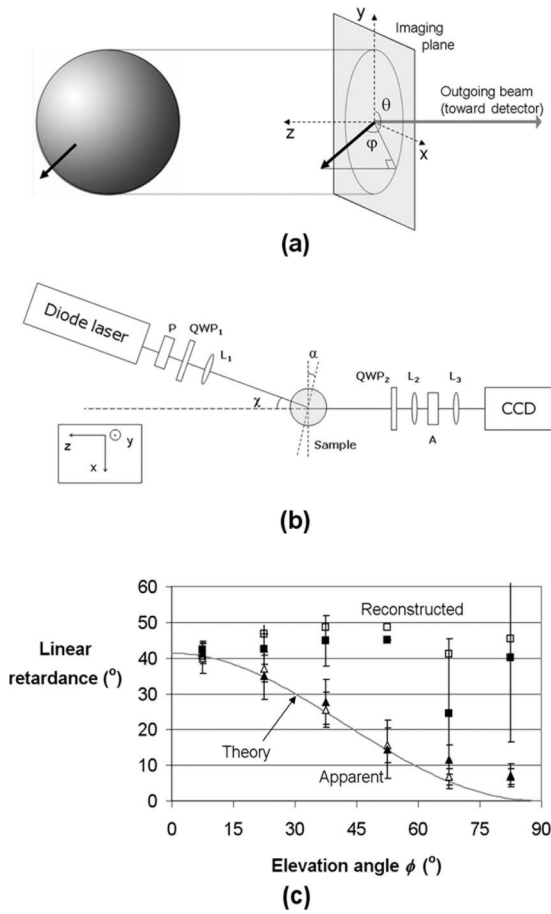
$$\delta_A = \delta' \cdot F(\varphi_A) = \delta' \cdot F\left(\tan^{-1}\left(\frac{u_z}{\sqrt{u_x^2 + u_y^2}}\right)\right);$$

$$\theta_A = \tan^{-1}\left(\frac{u_y}{u_x}\right)$$

$$\delta_B = \delta' \cdot F(\varphi_B) = \delta' \cdot F\left(\tan^{-1}\left(\frac{u'_z}{\sqrt{u_x'^2 + u_y'^2}}\right)\right); \quad (3)$$

$$\theta_B = \tan^{-1}\left(\frac{u'_y}{u'_x}\right).$$

Because $\mathbf{u}'$ is $\mathbf{u}$ rotated around the y axis by α, we can express Eq. (3) in terms of three unknown parameters: $\delta_x = \delta' \cdot u_x$, $\delta_y = \delta' \cdot u_y$, and $\delta_z = \delta' \cdot u_z$, and obtain the corresponding best fit. The resultant reconstructed linear retardance, $\delta' = \sqrt{\delta_x^2 + \delta_y^2 + \delta_z^2}$, is independent of the experimental geometry and should reflect intrinsic sample anisotropy.

Dual-projection reconstructions were performed for 39 different positions of the sphere anisotropy axis (19 and 20 reconstructions, respectively, with the on-axis and off-axis incident beams). Figure 1(c) shows a comparison the apparent (δ_{app}) and reconstructed (δ') linear retardance, with points in each 15° interval averaged together. The apparent δ_{app} values follow the theoretical dependence on the elevation angle δ [Eq. (1)] until φ reaches $\approx 70°$, at which point it plateaus around 6°. This is most likely due to imprecision on the positioning or alignment of the polarizers, or to ambient light scattering off the sphere. The average reconstructed linear retardance was $\bar{\delta}' = 41.4° \pm 7.5°$, which corresponds quite well to δ_{app} values measured when the anisotropy axis and probing beam are perpendicular ($\varphi = 0°$), when we expect $\delta_{app} = \delta'$: six measurements were made in this orientation with a mean value of $41.8° \pm 4.3°$. A comparison with the apparent linear retardance shows that the reconstructed linear retardance is a much more consistent and geometry-independent indicator of anisotropy. Furthermore, the average angle error (the angle $0° \le \beta \le 90°$ between the known and the reconstructed anisotropy axis) for all positions was $\bar{\beta} = 9.0° \pm 8.5°$, showing good correspondence with the visually established anisotropy axis.

To investigate the effect of different sample/beam geometries on the performance of the dual-projection reconstruction, we obtained the relative deviation, $\Delta\delta_i' = |\delta_i' - \bar{\delta}'|/\bar{\delta}'$ (where the average reconstructed linear retardance $\bar{\delta}'$ was taken as a measure of the "true" linear retardance) and angle error β for each reconstruction (data not shown). Both the magnitude of the reconstructed linear retardance and the orientation of the anisotropy axis were relatively consistent for all on-axis ($\chi = 0°$) reconstructions, with $1\% \le \Delta\delta' \le 17\%$ and $6° \le \beta \le 12°$, but a significantly larger error appears for angles of $\varphi > \approx 70°$ in the off-axis case ($\chi = 8°$), with $\beta \ge 25°$ and $\delta' \ge 50\%$. (There was no trend as to whether the reconstructed value was higher or lower than $\bar{\delta}'$.) This is consistent with our expectations: results from Fig. 1(c) suggest that δ_{app} deviates from theory for $\varphi > \approx 70°$, at which point the reconstruction (which relies on the theoretical relationship
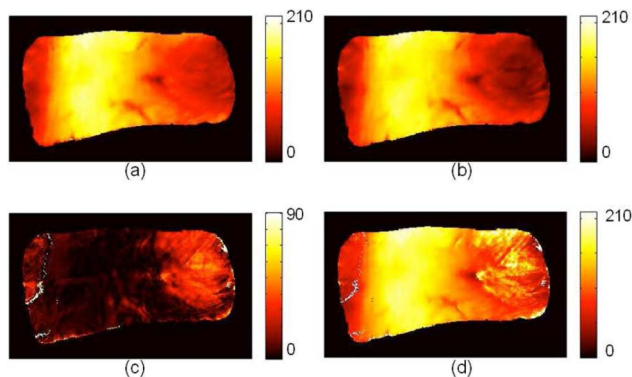

Fig. 1. (a) Relative geometry of the sphere anisotropy axis (dark arrow) and the probing beam. The elevation angle φ is the angle between the anisotropy axis and the imaging plane (xy plane); the azimuthal angle θ is the orientation of the projection of the anisotropy axis on the imaging plane. Only the outgoing beam is shown for clarity. (b) Schematic of the polarimetry imaging system: imaging is done with two different positions of the sphere, separated by a rotation of α about the vertical (y) axis. P, polarizer; L_i, lenses; QWP_i, quarter-wave plate; A, analyzer. The incident beam is either on axis or off axis by χ (shown here). (c) Apparent and reconstructed linear retardance for different elevation angles φ, and theoretical apparent linear retardance [Eq. (2)] for a sphere with real linear retardance $\delta = 41.4°$. Hollow markers, on axis ($\chi = 0°$); solid markers, off axis ($\chi = 8°$).

$$\delta_{app} = \frac{2\pi}{\lambda} \cdot d \cdot \Delta n \cdot \frac{\left[\left(\frac{n_o}{n_e}\right)^2 \cos^2\varphi + \sin^2\varphi\right]^{-1/2} - 1}{\frac{n_e}{n_o} - 1},$$

$$\delta_{app} = \frac{2\pi}{\lambda} \cdot d \cdot \Delta n \cdot F\left(\frac{n_e}{n_o}, \varphi\right), \quad (2)$$

where we have expressed the ratio $\Delta n_{app}/\Delta n$ as a function of n_e/n_o and φ. Because F is a slowly varying function of n_e/n_o over the physically relevant range, $F \approx f(\varphi)$ only. If $\mathbf{u}$ is the unitary vector in the direction of the anisotropy axis at the initial position A, $\mathbf{u}'$ is the unitary vector in the direction of the anisotropy axis at the rotated position B, and $\delta' = (2\pi/\lambda) \cdot d \cdot \Delta n$, there results

Fig. 2. (Color online) Apparent linear retardance δ_{app} (°) of a pig septum sample at (a) $\chi = 0°$ and (b) $\chi = 22°$. (c) Elevation angle φ. (d) Reconstructed linear retardance δ'. Field of view for all: 17 mm × 10 mm.

between δ_{app} and φ) would be expected to break down because of poor signal-to-noise ratio. Note that the value of α was found to have no influence on the performance of the reconstruction.

To determine whether this method produced acceptable results in more complex biological tissues, we performed dual-projection reconstruction in an axial, 500-μm-thick portion of healthy porcine myocardium (from the septum), interrogated off axis at $\chi = 22°$ (Fig. 2). (This larger angle was necessary to avoid direct light saturating the CCD). The apparent linear retardance δ_{app} and azimuthal angle θ (not shown), as corrected for phase wrap-around (see, [10]), were found for two positions of the tissue slab: with the sample plane perpendicular to the outgoing beam [Fig. 2(a)] and then rotated by $\alpha = 15°$ about the vertical (y) axis [Fig. 2(b)]. These were used to determine both the elevation angle φ [Fig. 2(c)] and the reconstructed linear retardance δ' [Fig. 2(d)]. The δ_{app} values [Figs. 2(a) and 2(b)] follow a low–high–low pattern from wall to wall (left to right), but dual-projection reconstruction [Figs. 2(c) and 2(d)] reveals that on the right-hand side, the low δ_{app} values are due to the high elevation angle (so that the reconstructed δ' values are comparable to those in the center), while on the left-most region, the low δ_{app} values are due to lower intrinsic anisotropy (so that the reconstructed δ' are lower than those in the center and right regions). The reconstructed δ' values thus provide a more intrinsic indicator of the tissue anisotropy, which, combined with knowledge of the anisotropy axis orientation, yield better insight into tissue structure.

In conclusion, we have demonstrated that the dual-projection reconstruction method can (1) account for the effect of the sample/beam geometry to yield a consistent indicator of tissue anisotropy, and (2) provide information about the true anisotropy axis orientation. Furthermore, we have verified that the off-axis imaging geometry of the probing beam introduces only a small error in the reconstruction. Further studies will be required to evaluate the effect of different incident beam directions (e.g., off-axis angles larger than 8°), to determine if improvement can be obtained using more than two projections, as well as to address the formidable challenges associated with nonuniaxial tissues. The information provided by this method about both the magnitude and the orientation of tissue anisotropy could prove useful in investigations of diseased and treated tissue structure, for example, to assess injury severity or therapy success in infarcted myocardium, where scar formation lowers tissue anisotropy and ventricular remodeling alters muscle fiber alignment.

References

1. J. Ramella-Roman, K. Lee, S. Prahl, and S. Jacques, J. Biomed Opt. **9**, 1305 (2004).
2. Z. Tannous, M. Al-Arashi, S. Shah, and A. Yaroslavsky, Lasers Surg. Med. **41**, 10 (2009).
3. P. Bagnaninchi, Y. Yang, M. Bonesi, G. Maffulli, C. Phelan, I. Meglinski, A. El Haj, and N. Naffulli, Phys. Med. Biol. **55**, 3777 (2010).
4. M. van Turnhout, S. Kranenbarg, and J. van Leeuwen, J. Biomed. Opt. **14**, 054018 (2009).
5. X. Li and G. Yao, Appl. Opt. **48**, 2625 (2009).
6. N. Ghosh, M. Wood, S. Li, R. Weisel, B. Wilson, R. Li, and I. A. Vitkin, J. Biophoton. **2**, 145 (2009).
7. M. Wood, N. Ghosh, M. A. Wallenburg, S. Li, R. Weisel, B. Wilson, R. Li, and I. A. Vitkin, "Polarization birefringence measurements for characterizing the myocardium, including healthy, infarcted and stem cell treated regenerating cardiac tissues," J. Biomed Opt. (to be published).
8. B. Saleh and M. Teich, *Fundamentals of Photonics*, 2nd ed. (Wiley-Interscience, 2007).
9. N. Ugryumova, J. Jacobs, M. Bonesi, and S. J. Matcher, Osteoarthr. Cartil. **17**, 33 (2009).
10. M. A. Wallenburg, M. Pop, M. Wood, N. Ghosh, G. A. Wright, and I. A. Vitkin, J. Innov. Opt. Health Sci. **3**, 109 (2010).
11. N. Ghosh, M. Wood, and I. A. Vitkin, J. Biomed. Opt. **13**, 044036 (2008).